DESY–06–241
December 2006

Jet-radius dependence of inclusive-jet cross sections in deep inelastic scattering at HERA

ZEUS Collaboration

Abstract

Differential inclusive-jet cross sections have been measured for different jet radii in neutral current deep inelastic ep scattering for boson virtualities $Q^2 > 125$ GeV^2 with the ZEUS detector at HERA using an integrated luminosity of 81.7 pb^{-1}. Jets were identified in the Breit frame using the k_T cluster algorithm in the longitudinally inclusive mode for different values of the jet radius R. Differential cross sections are presented as functions of Q^2 and the jet transverse energy, $E^{\rm jet}_{T,{\rm B}}$. The dependence on R of the inclusive-jet cross section has been measured for $Q^2 > 125$ and 500 GeV^2 and found to be linear with R in the range studied. Next-to-leading-order QCD calculations give a good description of the measurements for $0.5 \leq R \leq 1$. A value of $\alpha_s(M_Z)$ has been extracted from the measurements of the inclusive-jet cross-section $d\sigma/dQ^2$ with $R = 1$ for $Q^2 > 500$ GeV^2: $\alpha_s(M_Z) = 0.1207 \pm 0.0014$ (stat.) $^{+0.0035}_{-0.0033}$ (exp.) $^{+0.0022}_{-0.0023}$ (th.). The variation of α_s with $E^{\rm jet}_{T,{\rm B}}$ is in good agreement with the running of α_s as predicted by QCD.

The ZEUS Collaboration

S. Chekanov[1], M. Derrick, S. Magill, S. Miglioranzi[2], B. Musgrave, D. Nicholass[2], J. Repond, R. Yoshida
Argonne National Laboratory, Argonne, Illinois 60439-4815, USA [n]

M.C.K. Mattingly
Andrews University, Berrien Springs, Michigan 49104-0380, USA

M. Jechow, N. Pavel †, A.G. Yagües Molina
Institut für Physik der Humboldt-Universität zu Berlin, Berlin, Germany

S. Antonelli, P. Antonioli, G. Bari, M. Basile, L. Bellagamba, M. Bindi, D. Boscherini, A. Bruni, G. Bruni, L. Cifarelli, F. Cindolo, A. Contin, M. Corradi[3], S. De Pasquale, G. Iacobucci, A. Margotti, R. Nania, A. Polini, L. Rinaldi, G. Sartorelli, A. Zichichi
University and INFN Bologna, Bologna, Italy [e]

D. Bartsch, I. Brock, S. Goers[4], H. Hartmann, E. Hilger, H.-P. Jakob, M. Jüngst, O.M. Kind, E. Paul[5], J. Rautenberg[6], R. Renner, U. Samson, V. Schönberg, R. Shehzadi, M. Wang[7], M. Wlasenko
Physikalisches Institut der Universität Bonn, Bonn, Germany [b]

N.H. Brook, G.P. Heath, J.D. Morris, T. Namsoo
H.H. Wills Physics Laboratory, University of Bristol, Bristol, United Kingdom [m]

M. Capua, S. Fazio, A. Mastroberardino, M. Schioppa, G. Susinno, E. Tassi
Calabria University, Physics Department and INFN, Cosenza, Italy [e]

J.Y. Kim[8], K.J. Ma[9]
Chonnam National University, Kwangju, South Korea [g]

Z.A. Ibrahim, B. Kamaluddin, W.A.T. Wan Abdullah
Jabatan Fizik, Universiti Malaya, 50603 Kuala Lumpur, Malaysia [r]

Y. Ning, Z. Ren, F. Sciulli
Nevis Laboratories, Columbia University, Irvington on Hudson, New York 10027 [o]

J. Chwastowski, A. Eskreys, J. Figiel, A. Galas, M. Gil, K. Olkiewicz, P. Stopa, L. Zawiejski
The Henryk Niewodniczanski Institute of Nuclear Physics, Polish Academy of Sciences, Cracow, Poland [i]

L. Adamczyk, T. Bołd, I. Grabowska-Bołd, D. Kisielewska, J. Łukasik, M. Przybycień, L. Suszycki
Faculty of Physics and Applied Computer Science, AGH-University of Science and Technology, Cracow, Poland [p]

A. Kotański[10], W. Słomiński
Department of Physics, Jagellonian University, Cracow, Poland

V. Adler, U. Behrens, I. Bloch, A. Bonato, K. Borras, N. Coppola, J. Fourletova, A. Geiser, D. Gladkov, P. Göttlicher[11], I. Gregor, T. Haas, W. Hain, C. Horn, B. Kahle, U. Kötz, H. Kowalski, E. Lobodzinska, B. Löhr, R. Mankel, I.-A. Melzer-Pellmann, A. Montanari, D. Notz, A.E. Nuncio-Quiroz, R. Santamarta, U. Schneekloth, A. Spiridonov[12], H. Stadie, U. Stösslein, D. Szuba[13], J. Szuba[14], T. Theedt, G. Wolf, K. Wrona, C. Youngman, W. Zeuner
Deutsches Elektronen-Synchrotron DESY, Hamburg, Germany

W. Lohmann, S. Schlenstedt
Deutsches Elektronen-Synchrotron DESY, Zeuthen, Germany

G. Barbagli, E. Gallo, P. G. Pelfer
University and INFN, Florence, Italy [e]

A. Bamberger, D. Dobur, F. Karstens, N.N. Vlasov[15]
Fakultät für Physik der Universität Freiburg i.Br., Freiburg i.Br., Germany [b]

P.J. Bussey, A.T. Doyle, W. Dunne, J. Ferrando, D.H. Saxon, I.O. Skillicorn
Department of Physics and Astronomy, University of Glasgow, Glasgow, United Kingdom [m]

I. Gialas[16]
Department of Engineering in Management and Finance, Univ. of Aegean, Greece

T. Gosau, U. Holm, R. Klanner, E. Lohrmann, H. Salehi, P. Schleper, T. Schörner-Sadenius, J. Sztuk, K. Wichmann, K. Wick
Hamburg University, Institute of Exp. Physics, Hamburg, Germany [b]

C. Foudas, C. Fry, K.R. Long, A.D. Tapper
Imperial College London, High Energy Nuclear Physics Group, London, United Kingdom [m]

M. Kataoka[17], T. Matsumoto, K. Nagano, K. Tokushuku[18], S. Yamada, Y. Yamazaki
Institute of Particle and Nuclear Studies, KEK, Tsukuba, Japan [f]

A.N. Barakbaev, E.G. Boos, A. Dossanov, N.S. Pokrovskiy, B.O. Zhautykov
Institute of Physics and Technology of Ministry of Education and Science of Kazakhstan, Almaty, Kazakhstan

D. Son
Kyungpook National University, Center for High Energy Physics, Daegu, South Korea [g]

J. de Favereau, K. Piotrzkowski
Institut de Physique Nucléaire, Université Catholique de Louvain, Louvain-la-Neuve, Belgium [q]

F. Barreiro, C. Glasman[19], M. Jimenez, L. Labarga, J. del Peso, E. Ron, M. Soares, J. Terrón, M. Zambrana
Departamento de Física Teórica, Universidad Autónoma de Madrid, Madrid, Spain [l]

F. Corriveau, C. Liu, R. Walsh, C. Zhou
Department of Physics, McGill University, Montréal, Québec, Canada H3A 2T8 [a]

T. Tsurugai
Meiji Gakuin University, Faculty of General Education, Yokohama, Japan [f]

A. Antonov, B.A. Dolgoshein, I. Rubinsky, V. Sosnovtsev, A. Stifutkin, S. Suchkov
Moscow Engineering Physics Institute, Moscow, Russia [j]

R.K. Dementiev, P.F. Ermolov, L.K. Gladilin, I.I. Katkov, L.A. Khein, I.A. Korzhavina, V.A. Kuzmin, B.B. Levchenko[20], O.Yu. Lukina, A.S. Proskuryakov, L.M. Shcheglova, D.S. Zotkin, S.A. Zotkin
Moscow State University, Institute of Nuclear Physics, Moscow, Russia [k]

I. Abt, C. Büttner, A. Caldwell, D. Kollar, W.B. Schmidke, J. Sutiak
Max-Planck-Institut für Physik, München, Germany

G. Grigorescu, A. Keramidas, E. Koffeman, P. Kooijman, A. Pellegrino, H. Tiecke, M. Vázquez[17], L. Wiggers
NIKHEF and University of Amsterdam, Amsterdam, Netherlands [h]

N. Brümmer, B. Bylsma, L.S. Durkin, A. Lee, T.Y. Ling
Physics Department, Ohio State University, Columbus, Ohio 43210 [n]

P.D. Allfrey, M.A. Bell, A.M. Cooper-Sarkar, A. Cottrell, R.C.E. Devenish, B. Foster, K. Korcsak-Gorzo, S. Patel, V. Roberfroid[21], A. Robertson, P.B. Straub, C. Uribe-Estrada, R. Walczak
Department of Physics, University of Oxford, Oxford United Kingdom [m]

P. Bellan, A. Bertolin, R. Brugnera, R. Carlin, R. Ciesielski, F. Dal Corso, S. Dusini, A. Garfagnini, S. Limentani, A. Longhin, L. Stanco, M. Turcato
Dipartimento di Fisica dell' Università and INFN, Padova, Italy [e]

B.Y. Oh, A. Raval, J. Ukleja[22], J.J. Whitmore[23]
Department of Physics, Pennsylvania State University, University Park, Pennsylvania 16802 [o]

Y. Iga
Polytechnic University, Sagamihara, Japan [f]

G. D'Agostini, G. Marini, A. Nigro
Dipartimento di Fisica, Università 'La Sapienza' and INFN, Rome, Italy [e]

J.E. Cole, J.C. Hart
Rutherford Appleton Laboratory, Chilton, Didcot, Oxon, United Kingdom [m]

H. Abramowicz[24], A. Gabareen, R. Ingbir, S. Kananov, A. Levy
Raymond and Beverly Sackler Faculty of Exact Sciences, School of Physics, Tel-Aviv University, Tel-Aviv, Israel [d]

M. Kuze
Department of Physics, Tokyo Institute of Technology, Tokyo, Japan [f]

R. Hori, S. Kagawa[25], N. Okazaki, S. Shimizu, T. Tawara
Department of Physics, University of Tokyo, Tokyo, Japan [f]

R. Hamatsu, H. Kaji[26], S. Kitamura[27], O. Ota, Y.D. Ri
Tokyo Metropolitan University, Department of Physics, Tokyo, Japan [f]

M.I. Ferrero, V. Monaco, R. Sacchi, A. Solano
Università di Torino and INFN, Torino, Italy [e]

M. Arneodo, M. Ruspa
Università del Piemonte Orientale, Novara, and INFN, Torino, Italy [e]

S. Fourletov, J.F. Martin
Department of Physics, University of Toronto, Toronto, Ontario, Canada M5S 1A7 [a]

S.K. Boutle[16], J.M. Butterworth, C. Gwenlan[28], T.W. Jones, J.H. Loizides, M.R. Sutton[28], C. Targett-Adams, M. Wing
Physics and Astronomy Department, University College London, London, United Kingdom [m]

B. Brzozowska, J. Ciborowski[29], G. Grzelak, P. Kulinski, P. Łużniak[30], J. Malka[30], R.J. Nowak, J.M. Pawlak, T. Tymieniecka, A. Ukleja[31], A.F. Żarnecki
Warsaw University, Institute of Experimental Physics, Warsaw, Poland

M. Adamus, P. Plucinski[32]
Institute for Nuclear Studies, Warsaw, Poland

Y. Eisenberg, I. Giller, D. Hochman, U. Karshon, M. Rosin
Department of Particle Physics, Weizmann Institute, Rehovot, Israel [c]

E. Brownson, T. Danielson, A. Everett, D. Kçira, D.D. Reeder, P. Ryan, A.A. Savin, W.H. Smith, H. Wolfe
Department of Physics, University of Wisconsin, Madison, Wisconsin 53706, USA [n]

S. Bhadra, C.D. Catterall, Y. Cui, G. Hartner, S. Menary, U. Noor, J. Standage, J. Whyte
Department of Physics, York University, Ontario, Canada M3J 1P3 [a]

[1] supported by DESY, Germany
[2] also affiliated with University College London, UK
[3] also at University of Hamburg, Germany, Alexander von Humboldt Fellow
[4] self-employed
[5] retired
[6] now at Univ. of Wuppertal, Germany
[7] now at University of Regina, Canada
[8] supported by Chonnam National University in 2005
[9] supported by a scholarship of the World Laboratory Björn Wiik Research Project
[10] supported by the research grant no. 1 P03B 04529 (2005-2008)
[11] now at DESY group FEB, Hamburg, Germany
[12] also at Institut of Theoretical and Experimental Physics, Moscow, Russia
[13] also at INP, Cracow, Poland
[14] on leave of absence from FPACS, AGH-UST, Cracow, Poland
[15] partly supported by Moscow State University, Russia
[16] also affiliated with DESY
[17] now at CERN, Geneva, Switzerland
[18] also at University of Tokyo, Japan
[19] Ramón y Cajal Fellow
[20] partly supported by Russian Foundation for Basic Research grant no. 05-02-39028-NSFC-a
[21] EU Marie Curie Fellow
[22] partially supported by Warsaw University, Poland
[23] This material was based on work supported by the National Science Foundation, while working at the Foundation.
[24] also at Max Planck Institute, Munich, Germany, Alexander von Humboldt Research Award
[25] now at KEK, Tsukuba, Japan
[26] now at Nagoya University, Japan
[27] Department of Radiological Science
[28] PPARC Advanced fellow
[29] also at Łódź University, Poland
[30] Łódź University, Poland
[31] supported by the Polish Ministry for Education and Science grant no. 1 P03B 12629
[32] supported by the Polish Ministry for Education and Science grant no. 1 P03B 14129

[†] deceased

[a] supported by the Natural Sciences and Engineering Research Council of Canada (NSERC)

[b] supported by the German Federal Ministry for Education and Research (BMBF), under contract numbers HZ1GUA 2, HZ1GUB 0, HZ1PDA 5, HZ1VFA 5

[c] supported in part by the MINERVA Gesellschaft für Forschung GmbH, the Israel Science Foundation (grant no. 293/02-11.2) and the U.S.-Israel Binational Science Foundation

[d] supported by the German-Israeli Foundation and the Israel Science Foundation

[e] supported by the Italian National Institute for Nuclear Physics (INFN)

[f] supported by the Japanese Ministry of Education, Culture, Sports, Science and Technology (MEXT) and its grants for Scientific Research

[g] supported by the Korean Ministry of Education and Korea Science and Engineering Foundation

[h] supported by the Netherlands Foundation for Research on Matter (FOM)

[i] supported by the Polish State Committee for Scientific Research, grant no. 620/E-77/SPB/DESY/P-03/DZ 117/2003-2005 and grant no. 1P03B07427/2004-2006

[j] partially supported by the German Federal Ministry for Education and Research (BMBF)

[k] supported by RF Presidential grant N 1685.2003.2 for the leading scientific schools and by the Russian Ministry of Education and Science through its grant for Scientific Research on High Energy Physics

[l] supported by the Spanish Ministry of Education and Science through funds provided by CICYT

[m] supported by the Particle Physics and Astronomy Research Council, UK

[n] supported by the US Department of Energy

[o] supported by the US National Science Foundation. Any opinion, findings and conclusions or recommendations expressed in this material are those of the authors and do not necessarily reflect the views of the National Science Foundation.

[p] supported by the Polish Ministry of Science and Higher Education

[q] supported by FNRS and its associated funds (IISN and FRIA) and by an Inter-University Attraction Poles Programme subsidised by the Belgian Federal Science Policy Office

[r] supported by the Malaysian Ministry of Science, Technology and Innovation/Akademi Sains Malaysia grant SAGA 66-02-03-0048

1 Introduction

The study of jet production in ep collisions at HERA has been well established as a testing ground of perturbative QCD (pQCD) providing precise determinations of the strong coupling constant, α_s, and its scale dependence. The jet observables used to test pQCD included dijet [1–4], inclusive-jet [2, 4–6] and multijet [7, 8] cross sections in neutral current (NC) deep inelastic ep scattering (DIS), dijet [9–13], inclusive-jet [14, 15] and multijet [16] cross sections in photoproduction and the internal structure of jets in NC [17–19] and charged current [20] DIS.

These studies demonstrated that the k_T cluster algorithm [21] in the longitudinally invariant inclusive mode [22] is at present the method to reconstruct jets in ep collisions for which the smallest uncertainties are achieved. Previous analyses were done with jet radius $R = 1$, where R is the maximum distance in the pseudorapidity (η) - azimuth (ϕ) plane for particle recombination. The study of the predicted jet cross sections using different jet radii allows the identification of the values of R for which the theory is most reliable. Furthermore, smaller values of the jet radius R are of particular interest for the identification of heavy particles decaying into jets; in these decays, the final-state jets may emerge close in phase space and need to be identified separately for a faithful reconstruction of the properties of the parent particle [23]. Neutral current DIS provides a well understood environment in which to study the dependence of jet production on the jet radius and to confront the data with precise next-to-leading-order (NLO) QCD calculations in a hadron-induced reaction.

The hadronic final state in NC DIS may consist of jets of high transverse energy, E_T^{jet}, produced in the hard-scattering process. In NC DIS, the Breit frame [24] is preferred to conduct the jet search, since jet production is directly sensitive to hard QCD processes; in the Born process ($eq \to eq$), the virtual boson (V^*, with $V^* = \gamma, Z$) is absorbed by the struck quark, which is back-scattered with zero transverse momentum with respect to the V^* direction. At leading order (LO) in α_s, the boson-gluon-fusion ($V^*g \to q\bar{q}$) and QCD-Compton ($V^*q \to qg$) processes give rise to two hard jets with opposite transverse momenta. Inclusive-jet production at high E_T^{jet} allows more stringent tests of the pQCD calculations than dijet production due to the reduced theoretical uncertainties. Restrictions on the topology of dijet events are necessary to avoid infrared-sensitive regions where the NLO QCD programs are not reliable, whereas inclusive-jet cross sections are infrared insensitive. Therefore, such measurements allow tests of pQCD in the widest phase-space region for jet production. In particular, previous measurements of inclusive-jet cross sections in NC DIS at high Q^2 [5], where Q^2 is the negative of the square of the four-momentum transfer, provided the most precise determination of α_s at HERA to date.

This letter presents new measurements of differential inclusive-jet cross sections as a function of the jet transverse energy in the Breit frame, $E_{T,\mathrm{B}}^{\mathrm{jet}}$, and Q^2 for different values of R. For $R = 1$, this analysis is based on the same inclusive-jet data sample presented in a recent publication [4]. The results have been compared with NLO QCD calculations using recent parameterisations of the parton distribution functions (PDFs) of the proton [25–27]. In addition, an updated determination of α_s and of its scale dependence has been obtained using a data sample which corresponds to more than a twofold increase in luminosity with respect to the previous analysis [5].

2 Experimental set-up

A detailed description of the ZEUS detector can be found elsewhere [28, 29]. A brief outline of the components that are most relevant for this analysis is given below.

Charged particles are tracked in the central tracking detector (CTD) [30], which operates in a magnetic field of 1.43 T provided by a thin superconducting solenoid. The CTD consists of 72 cylindrical drift-chamber layers, organised in nine superlayers covering the polar-angle[1] region $15^\circ < \theta < 164^\circ$. The transverse-momentum resolution for full-length tracks can be parameterised as $\sigma(p_T)/p_T = 0.0058p_T \oplus 0.0065 \oplus 0.0014/p_T$, with p_T in GeV. The tracking system was used to measure the interaction vertex with a typical resolution along (transverse to) the beam direction of 0.4 (0.1) cm and to cross-check the energy scale of the calorimeter.

The high-resolution uranium–scintillator calorimeter (CAL) [31] covers 99.7% of the total solid angle and consists of three parts: the forward (FCAL), the barrel (BCAL) and the rear (RCAL) calorimeters. Each part is subdivided transversely into towers and longitudinally into one electromagnetic section and either one (in RCAL) or two (in BCAL and FCAL) hadronic sections. The smallest subdivision of the calorimeter is called a cell. Under test-beam conditions, the CAL single-particle relative energy resolutions were $\sigma(E)/E = 0.18/\sqrt{E}$ for electrons and $\sigma(E)/E = 0.35/\sqrt{E}$ for hadrons, with E in GeV.

The luminosity was measured from the rate of the bremsstrahlung process $ep \to e\gamma p$. The resulting small-angle energetic photons were measured by the luminosity monitor [32], a lead-scintillator calorimeter placed in the HERA tunnel at $Z = -107$ m.

[1] The ZEUS coordinate system is a right-handed Cartesian system, with the Z axis pointing in the proton beam direction, referred to as the "forward direction", and the X axis pointing left towards the centre of HERA. The coordinate origin is at the nominal interaction point.

3 Data selection and jet search

The data were collected during the running period 1998-2000, when HERA operated with protons of energy $E_p = 920$ GeV and electrons or positrons[2] of energy $E_e = 27.5$ GeV, and correspond to an integrated luminosity of 81.7 ± 1.8 pb^{-1}, of which 16.7 pb^{-1} (65.0 pb^{-1}) was for e^-p (e^+p) collisions.

Neutral current DIS events were selected offline using the same criteria as reported in a recent publication [4]. The main steps are briefly listed below.

The scattered-electron candidate was identified from the pattern of energy deposits in the CAL [33]. The energy (E'_e) and polar angle (θ_e) of the electron candidate were determined from the CAL measurements. The Q^2 variable was reconstructed using the double angle method ($Q^2_{\rm DA}$) [34]. The angle γ_h, which corresponds to the angle of the scattered quark in the quark-parton model, was reconstructed using the hadronic final state [34].

The main requirements imposed on the data sample were: an electron candidate with $E'_e > 10$ GeV; a vertex position along the beam axis in the range $|Z| < 34$ cm; $38 < (E - P_Z) < 65$ GeV, where E is the total energy as measured by the CAL, $E = \sum_i E_i$, and P_Z is the Z-component of the vector $\boldsymbol{P} = \sum_i E_i \boldsymbol{r_i}$; in both cases the sum runs over all CAL cells, E_i is the energy of the CAL cell i and $\boldsymbol{r_i}$ is a unit vector along the line joining the reconstructed vertex and the geometric centre of the cell i; $Q^2 > 125$ GeV^2; and $|\cos\gamma_h| < 0.65$. After all these requirements, contamination from non-ep interactions and other physics processes was negligible.

The k_T cluster algorithm was used in the longitudinally invariant inclusive mode to reconstruct jets in the hadronic final state both in data and in Monte Carlo (MC) simulated events (see Section 4). In the data, the algorithm was applied to the energy deposits measured in the CAL cells after excluding those associated with the scattered-electron candidate. In the following discussion, $E^i_{T,\rm B}$ denotes the transverse energy, $\eta^i_{\rm B}$ the pseudorapidity and $\phi^i_{\rm B}$ the azimuthal angle of object i in the Breit frame. For each pair of objects, where the initial objects are the energy deposits in the CAL cells, the quantity

$$d_{ij} = \min(E^i_{T,\rm B}, E^j_{T,\rm B})^2 \cdot [(\eta^i_{\rm B} - \eta^j_{\rm B})^2 + (\phi^i_{\rm B} - \phi^j_{\rm B})^2]/R^2$$

was calculated. For each individual object, the quantity $d_i = (E^i_{T,\rm B})^2$ was also calculated. If, of all the values $\{d_{ij}, d_i\}$, d_{kl} was the smallest, then objects k and l were combined into a single new object. If, however, d_k was the smallest, then object k was considered a jet and was removed from the sample. The procedure was repeated until all objects were

[2] Here and in the following, the term "electron" denotes generically both the electron (e^-) and the positron (e^+).

assigned to jets. The jet search was performed with different jet radii ($R = 0.5$, 0.7 and 1) and the jet variables were defined according to the Snowmass convention [35].

After reconstructing the jet variables in the Breit frame, the massless four-momenta were boosted into the laboratory frame, where the transverse energy ($E^{\rm jet}_{T,\rm LAB}$) and the pseudorapidity ($\eta^{\rm jet}_{\rm LAB}$) of each jet were calculated. Energy corrections [5,11,18] were then applied to the jets in the laboratory frame and propagated back into $E^{\rm jet}_{T,\rm B}$. The jet variables in the laboratory frame were also used to apply additional cuts on the selected sample, as explained in a recent publication [4]: events were removed from the sample if any of the jets was in the backward region of the detector ($\eta^{\rm jet}_{\rm LAB} < -2$) and jets were not included in the final sample if $E^{\rm jet}_{T,\rm LAB} < 2.5$ GeV.

Only events with at least one jet in the pseudorapidity range $-2 < \eta^{\rm jet}_{\rm B} < 1.5$ were kept for further analysis. The final data samples with at least one jet satisfying $E^{\rm jet}_{T,\rm B} > 8$ GeV contained 19908 events for $R = 1$, 16231 for $R = 0.7$ and 12935 for $R = 0.5$.

4 Monte Carlo simulation

Samples of events were generated to determine the response of the detector to jets of hadrons and the correction factors necessary to obtain the hadron-level jet cross sections. The hadron level is defined by those hadrons with lifetime $\tau \geq 10$ ps. The generated events were passed through the GEANT 3.13-based [36] ZEUS detector- and trigger-simulation programs [29]. They were reconstructed and analysed by the same program chain as the data.

Neutral current DIS events including electroweak radiative effects were simulated using the HERACLES 4.6.1 [37] program with the DJANGOH 1.1 [38] interface to the QCD programs. The QCD cascade is simulated using the colour-dipole model (CDM) [39] including the leading-order (LO) QCD diagrams as implemented in ARIADNE 4.08 [40] and, alternatively, with the MEPS model of LEPTO 6.5 [41]. The CTEQ5D [42] parameterisations of the proton PDFs were used for these simulations. Fragmentation into hadrons is performed using the Lund string model [43] as implemented in JETSET [44, 45].

The jet search was performed on the MC events using the energy measured in the CAL cells in the same way as for the data. The same jet algorithm was also applied to the final-state particles (hadron level) and to the partons available after the parton shower (parton level). The MC programs were also used to correct the measured cross sections for QED radiative effects and the running of $\alpha_{\rm em}$.

5 QCD calculations

The measurements were compared with LO ($\mathcal{O}(\alpha_s)$) and NLO QCD ($\mathcal{O}(\alpha_s^2)$) calculations obtained using the program DISENT [46]. The calculations were performed in the $\overline{\rm MS}$ renormalisation and factorisation schemes using a generalised version [46] of the subtraction method [47]. The number of flavours was set to five and the renormalisation (μ_R) and factorisation (μ_F) scales were chosen to be $\mu_R = E_{T,\rm B}^{\rm jet}$ and $\mu_F = Q$, respectively. The strong coupling constant was calculated at two loops with $\Lambda^{(5)}_{\overline{\rm MS}} = 226$ MeV, corresponding to $\alpha_s(M_Z) = 0.118$. The calculations were performed using the ZEUS-S [25] parameterisations of the proton PDFs. In DISENT, the value of $\alpha_{\rm em}$ was fixed to 1/137. The k_T cluster algorithm was also applied to the partons in the events generated by DISENT in order to compute the jet cross-section predictions. The calculations were performed for the same values of R as for the data. In addition, predictions were obtained for $R = 0.3$ and 1.2 to determine the range of R in which the theory is most reliable.

Since the measurements refer to jets of hadrons, whereas the NLO QCD calculations refer to jets of partons, the predictions were corrected to the hadron level using the MC models. The multiplicative correction factor ($C_{\rm had}$) was defined as the ratio of the cross section for jets of hadrons over that for jets of partons, estimated by using the MC programs described in Section 4. The mean of the ratios obtained with ARIADNE and LEPTO-MEPS was taken as the value of $C_{\rm had}$. The value of $C_{\rm had}$ differs from unity by less than 5%, 15% and 25% for $R = 1$, 0.7 and 0.5, respectively, in the region $Q^2 \geq 500$ GeV^2. For $R = 1.2$, $C_{\rm had}$ differs from unity by less than 1% and for $R = 0.3$, $C_{\rm had}$ differs by 40%.

DISENT does not include the contribution from Z^0 exchange; MC simulated events with and without Z^0 exchange were used to include this effect in the NLO QCD predictions. In the following, NLO QCD calculations will refer to the fully corrected predictions, except where otherwise stated.

5.1 Theoretical uncertainties

Several sources of uncertainty in the theoretical predictions were considered:

- the uncertainty on the NLO QCD calculations due to terms beyond NLO, estimated by varying μ_R between $E_{T,\rm B}^{\rm jet}/2$ and $2E_{T,\rm B}^{\rm jet}$, was below $\pm 7\%$ at low Q^2 and low $E_{T,\rm B}^{\rm jet}$ and decreased to less than $\pm 5\%$ for $Q^2 > 250$ GeV^2 for $R = 1$. For smaller radii, the estimated uncertainty is smaller (higher) at low (high) Q^2 than for $R = 1$. For $R = 1.2$, this uncertainty increases up to $\pm 10\%$ for $Q^2 \approx 500$ GeV^2;
- the uncertainty on the NLO QCD calculations due to those on the proton PDFs was estimated by repeating the calculations using 22 additional sets from the ZEUS-S anal-

ysis, which takes into account the statistical and correlated systematic experimental uncertainties of each data set used in the determination of the proton PDFs. The resulting uncertainty in the cross sections was below $\pm 3\%$, except in the high-$E_{T,\mathrm{B}}^{\mathrm{jet}}$ region where it reached $\pm 4.4\%$;

- the uncertainty on the NLO QCD calculations due to that on $\alpha_s(M_Z)$ was estimated by repeating the calculations using two additional sets of proton PDFs, for which different values of $\alpha_s(M_Z)$ were assumed in the fits. The difference between the calculations using these various sets was scaled by a factor such as to reflect the uncertainty on the current world average of α_s [48]. The resulting uncertainty in the cross sections was below $\pm 2\%$;
- the uncertainty from the modelling of the QCD cascade was assumed to be half the difference between the hadronisation corrections obtained using the Ariadne and Lepto-MEPS models. The resulting uncertainty on the cross sections was less than 1.4% for $R = 1$ and increased up to $\sim 4\%$ for $R = 0.5$;
- the uncertainty of the calculations in the value of μ_F was estimated by repeating the calculations with $\mu_F = Q/2$ and $2Q$. The variation of the calculations was negligible.

The total theoretical uncertainty was obtained by adding in quadrature the individual uncertainties listed above.

It is concluded that NLO QCD provides predictions with comparable precision in the range $R = 0.5 - 1$. For larger values of R, e.g. $R = 1.2$, it was estimated that the uncertainty on the NLO QCD calculations due to terms beyond NLO increases up to about 10% for high Q^2 values. On the other hand, the hadronisation correction estimated for the cross sections with smaller radii, e.g. $R = 0.3$, increases up to about 40%. Therefore, only measurements for the range $R = 0.5 - 1$ are presented in Section 7.

6 Acceptance corrections

The $E_{T,\mathrm{B}}^{\mathrm{jet}}$ and Q^2 distributions in the data were corrected for detector effects using bin-by-bin correction factors determined with the MC samples. These correction factors took into account the efficiency of the trigger, the selection criteria and the purity and efficiency of the jet reconstruction. For this approach to be valid, the uncorrected distributions of the data must be well described by the MC simulations at the detector level. This condition was satisfied by both the Ariadne and Lepto-MEPS MC samples. The average between the acceptance-correction values obtained with Ariadne and Lepto-MEPS was used to correct the data to the hadron level. The deviations in the results obtained by using either Ariadne or Lepto-MEPS to correct the data from their average were taken to represent

systematic uncertainties of the effect of the QCD-cascade model in the corrections (see Section 6.1). The acceptance-correction factors differed from unity by typically less than 10%.

6.1 Experimental uncertainties

The following sources of systematic uncertainty were considered for the measured cross sections:

- the uncertainty in the absolute energy scale of the jets was estimated to be $\pm 1\%$ for $E^{\rm jet}_{T,\rm LAB} > 10$ GeV and $\pm 3\%$ for lower $E^{\rm jet}_{T,\rm LAB}$ values [10, 11, 49]. The resulting uncertainty was about $\pm 5\%$;

- the differences in the results obtained by using either ARIADNE or LEPTO-MEPS to correct the data for detector effects were taken to represent systematic uncertainties. The resulting uncertainty was typically below $\pm 3\%$;

- the uncertainty due to the selection cuts was estimated by varying the values of the cuts within the resolution of each variable; the effect on the cross sections was typically below $\pm 3\%$;

- the uncertainty on the reconstruction of the boost to the Breit frame was estimated by using the direction of the track associated to the scattered electron instead of that derived from its impact position in the CAL. The effect was typically below $\pm 1\%$;

- the uncertainty in the absolute energy scale of the electron candidate was estimated to be $\pm 1\%$ [50]. The resulting uncertainty was below $\pm 1\%$;

- the uncertainty in the cross sections due to that in the simulation of the trigger was negligible.

The systematic uncertainties not associated with the absolute energy scale of the jets were added in quadrature to the statistical uncertainties and are shown in the figures as error bars. The uncertainty due to the absolute energy scale of the jets is shown separately as a shaded band in each figure, due to the large bin-to-bin correlation. In addition, there was an overall normalisation uncertainty of 2.2% from the luminosity determination, which is not included in the figures.

7 Results

7.1 Inclusive-jet differential cross sections for different jet radii

The inclusive-jet differential cross sections were measured in the kinematic region $Q^2 > 125$ GeV^2 and $|\cos\gamma_h| < 0.65$. These cross sections include every jet of hadrons in the event with $E_{T,\mathrm{B}}^{\mathrm{jet}} > 8$ GeV and $-2 < \eta_{\mathrm{B}}^{\mathrm{jet}} < 1.5$ and were corrected for detector and QED radiative effects and the running of α_{em}.

The measurements of the inclusive-jet differential cross sections as functions of $E_{T,\mathrm{B}}^{\mathrm{jet}}$ and Q^2 are presented in Figs. 1a and 2a for jet radii $R = 1$, 0.7 and 0.5. In these figures, each data point is plotted at the abscissa at which the NLO QCD differential cross section was equal to its bin-averaged value. The measured $d\sigma/dE_{T,\mathrm{B}}^{\mathrm{jet}}$ ($d\sigma/dQ^2$) exhibits a steep fall-off over three (five) orders of magnitude for the jet radii considered in the $E_{T,\mathrm{B}}^{\mathrm{jet}}$ (Q^2) measured range.

The NLO QCD predictions with $\mu_R = E_{T,\mathrm{B}}^{\mathrm{jet}}$ are compared to the measurements in Figs. 1a and 2a. The fractional difference of the measured differential cross sections to the NLO QCD calculations is shown in Figs. 1b and 2b. The calculations reproduce the measured differential cross sections well for the jet radii considered, with similar precision. To study the scale dependence, NLO QCD calculations using $\mu_R = Q$ were also compared to the data (not shown); they also provide a good description of the data.

7.2 Dependence of the inclusive-jet cross section on the jet radius

Measurements of the inclusive-jet cross section have been performed for $E_{T,\mathrm{B}}^{\mathrm{jet}} > 8$ GeV and $-2 < \eta_{\mathrm{B}}^{\mathrm{jet}} < 1.5$ in the kinematic range given by $|\cos\gamma_h| < 0.65$ integrated above $Q^2_{\mathrm{min}} = 125$ and 500 GeV^2 for different jet radii. The measured cross section, σ_{jets}, as a function of R is presented in Figs. 3a and 3b. The measured cross sections increase linearly with R in the range between 0.5 and 1. The increase of σ_{jets} as R increases can be understood as the result of more transverse energy being gathered in a jet so that a larger number of jets has $E_{T,\mathrm{B}}^{\mathrm{jet}}$ exceeding the threshold of 8 GeV.

The predictions of LO and NLO QCD for σ_{jets} at the parton level, with no corrections for hadronisation or Z^0 exchange, are shown in the inset of Fig. 3. The LO predictions do not depend on R since there is only one parton per jet. The NLO calculations give the lowest-order contribution to the R dependence of the inclusive-jet cross section. The NLO QCD calculations, corrected to include hadronisation and Z^0 effects, are also shown in

the inset of Fig. 3. It is observed that, in addition to the effects due to parton radiation, the hadronisation corrections further modify the shape of the prediction.

The NLO QCD calculations are compared to the data in Fig. 3. They give a good description of the R dependence of the data within the jet-radius range considered. The uncertainty of the NLO calculation is also shown. The total theoretical uncertainty of the cross section integrated above $Q^2_{\rm min} = 125$ GeV^2 (500 GeV^2) changes from 5.6% (3.2%) for $R = 1$ to 4.2% (7.1%) for $R = 0.5$. This variation is due to a change of the uncertainty arising from higher-order QCD corrections and hadronisation. The uncertainties arising from $\alpha_s(M_Z)$ and the proton PDFs do not change significantly with R.

7.3 Determination of $\alpha_s(M_Z)$

The measured differential cross sections presented in Section 7.1 were used to determine a value of $\alpha_s(M_Z)$ using the method presented previously [5]. The NLO QCD calculations were performed using the program DISENT with five sets of ZEUS-S proton PDFs which were determined from global fits assuming different values of $\alpha_s(M_Z)$, namely $\alpha_s(M_Z) =$ 0.115, 0.117, 0.119, 0.121 and 0.123. The value of $\alpha_s(M_Z)$ used in each calculation was that associated with the corresponding set of PDFs. The $\alpha_s(M_Z)$ dependence of the predicted cross sections in each bin i of A ($A = Q^2, E^{\rm jet}_{T,{\rm B}}$) was parameterised according to

$$[d\sigma/dA(\alpha_s(M_Z))]_i = C_1^i \alpha_s(M_Z) + C_2^i \alpha_s^2(M_Z),$$

where C_1^i and C_2^i were determined from a χ^2 fit to the NLO QCD calculations. The value of $\alpha_s(M_Z)$ was determined by a χ^2 fit to the measured $d\sigma/dA$ values for several regions of the variable A. The values of $\alpha_s(M_Z)$ obtained from the various differential cross sections and jet radii were found to be consistent. The result obtained using the measured $d\sigma/dQ^2$ for $Q^2 > 500$ GeV^2 with $R = 1$ yields the smallest uncertainty and, therefore, represents the most precise determination from this analysis. In the region $Q^2 > 500$ GeV^2, the experimental systematic uncertainties on the cross sections are smaller than at lower Q^2 and the theoretical uncertainties due to the proton PDFs and to terms beyond NLO are minimised.

The uncertainties on the extracted values of $\alpha_s(M_Z)$ due to the experimental systematic uncertainties were evaluated by repeating the analysis for each systematic check presented in Section 6.1. The overall normalisation uncertainty from the luminosity determination was also considered. The largest contribution to the experimental uncertainty comes from the jet energy scale and amounts to $\pm 2\%$ on $\alpha_s(M_Z)$. The theoretical uncertainties were evaluated as described in Section 5.1. The largest contribution was the theoretical uncertainty arising from terms beyond NLO, which was estimated by using the method proposed by Jones et al. [51], and amounted to $\pm 1.5\%$. The uncertainty due to the proton

PDFs was $\pm 0.7\%$. The uncertainty arising from the hadronisation effects amounted to $\pm 0.8\%$.

As a cross-check, $\alpha_s(M_Z)$ was determined by using NLO QCD calculations based on the MRST2001 [26] and CTEQ6 [27] sets of proton PDFs. The values obtained are consistent within 1% with those based on ZEUS-S. The uncertainty arising from the proton PDFs was estimated to be $\pm 0.7\%$ ($\pm 1.6\%$) using the results of the MRST2001 (CTEQ6) analysis.

The value of $\alpha_s(M_Z)$ obtained from the measured $d\sigma/dQ^2$ for $Q^2 > 500$ GeV^2 with $R = 1$ is

$$\alpha_s(M_Z) = 0.1207 \pm 0.0014 \text{ (stat.)} \, ^{+0.0035}_{-0.0033} \text{ (exp.)} \, ^{+0.0022}_{-0.0023} \text{ (th.)}.$$

This value of $\alpha_s(M_Z)$ is consistent with the current world average of 0.1189 ± 0.0010 [48] as well as with the HERA average of 0.1186 ± 0.0051 [52]. It has a precision comparable to the values obtained from e^+e^- interactions [48].

7.4 Energy-scale dependence of α_s

The QCD prediction for the energy-scale dependence of the strong coupling constant was tested by determining α_s from the measured $d\sigma/dE^{\rm jet}_{T,\rm B}$ with $R = 1$ at different $E^{\rm jet}_{T,\rm B}$ values. The method employed was the same as described above, but parameterising the α_s dependence of $d\sigma/dE^{\rm jet}_{T,\rm B}$ in terms of $\alpha_s(\langle E^{\rm jet}_{T,\rm B}\rangle)$ instead of $\alpha_s(M_Z)$, where $\langle E^{\rm jet}_{T,\rm B}\rangle$ is the average $E^{\rm jet}_{T,\rm B}$ of the data in each bin. The extracted values of α_s are shown in Fig. 4. The results are in good agreement with the predicted running of the strong coupling constant [53] calculated at two loops [54] over a large range in $E^{\rm jet}_{T,\rm B}$.

8 Summary

Measurements of differential cross sections for inclusive-jet production in neutral current deep inelastic ep scattering at a centre-of-mass energy of 318 GeV have been presented. The cross sections refer to jets of hadrons identified in the Breit frame with the k_T cluster algorithm in the longitudinally invariant inclusive mode. The cross sections are given in the kinematic region of $Q^2 > 125$ GeV^2 and $|\cos\gamma_h| < 0.65$.

The dependence of the inclusive-jet cross sections on the jet-radius R has been studied. It has been determined that NLO QCD provides predictions with comparable precision in the range $R = 0.5 - 1$. Measurements of inclusive-jet differential cross sections for this jet-radius range have been presented. The NLO QCD calculations provide a good description of the measured inclusive-jet differential cross sections $d\sigma/dE^{\rm jet}_{T,\rm B}$ and $d\sigma/dQ^2$ for $R = 1$, 0.7 and 0.5. It is observed that the measured inclusive-jet cross section

integrated above $Q^2_{\rm min} = 125$ and 500 GeV^2 increases linearly with R in the jet-radius range studied.

The measured inclusive-jet differential cross sections have been used to extract a value of $\alpha_s(M_Z)$. A QCD fit of the cross-section $d\sigma/dQ^2$ with $R = 1$ for $Q^2 > 500$ GeV^2 yields the determination with smallest uncertainty,

$$\alpha_s(M_Z) = 0.1207 \pm 0.0014\ (\text{stat.})\ ^{+0.0035}_{-0.0033}\ (\text{exp.})\ ^{+0.0022}_{-0.0023}\ (\text{th.}).$$

This value is in good agreement with the world and HERA averages. The extracted values of α_s at different $E^{\rm jet}_{T,\rm B}$ are in good agreement with the predicted running of the strong coupling constant over a large range in $E^{\rm jet}_{T,\rm B}$.

Acknowledgements

We thank the DESY Directorate for their strong support and encouragement. The remarkable achievements of the HERA machine group were essential for the successful completion of this work and are greatly appreciated. We are grateful for the support of the DESY computing and network services. The design, construction and installation of the ZEUS detector have been made possible owing to the ingenuity and effort of many people who are not listed as authors.

References

[1] ZEUS Coll., J. Breitweg et al., Phys. Lett. B 507 (2001) 70.

[2] H1 Coll., C. Adloff et al., Eur. Phys. J. C 19 (2001) 289.

[3] ZEUS Coll., S. Chekanov et al., Eur. Phys. J. C 23 (2002) 13.

[4] ZEUS Coll., S. Chekanov et al., Preprint DESY-06-128 (hep-ex/0608048), DESY, 2006.

[5] ZEUS Coll., S. Chekanov et al., Phys. Lett. B 547 (2002) 164.

[6] ZEUS Coll., S. Chekanov et al., Phys. Lett. B 551 (2003) 226.

[7] H1 Coll., C. Adloff et al., Phys. Lett. B 515 (2001) 17.

[8] ZEUS Coll., S. Chekanov et al., Eur. Phys. J. C 44 (2005) 183.

[9] ZEUS Coll., J. Breitweg et al., Eur. Phys. J. C 11 (1999) 35.

[10] ZEUS Coll., S. Chekanov et al., Eur. Phys. J. C 23 (2002) 615.

[11] ZEUS Coll., S. Chekanov et al., Phys. Lett. B 531 (2002) 9.

[12] H1 Coll., C. Adloff et al., Eur. Phys. J. C 25 (2002) 13.

[13] H1 Coll., A. Aktas et al., Phys. Lett. B 639 (2006) 21.

[14] ZEUS Coll., S. Chekanov et al., Phys. Lett. B 560 (2003) 7.

[15] H1 Coll., C. Adloff et al., Eur. Phys. J. C 29 (2003) 497.

[16] ZEUS Coll., J. Breitweg et al., Phys. Lett. B 443 (1998) 394.

[17] H1 Coll., C. Adloff et al., Nucl. Phys. B 545 (1999) 3.

[18] ZEUS Coll., S. Chekanov et al., Phys. Lett. B 558 (2003) 41.

[19] ZEUS Coll., S. Chekanov et al., Nucl. Phys. B 700 (2004) 3.

[20] ZEUS Coll., S. Chekanov et al., Eur. Phys. J. C 31 (2003) 149.

[21] S. Catani et al., Nucl. Phys. B 406 (1993) 187.

[22] S.D. Ellis and D.E. Soper, Phys. Rev. D 48 (1993) 3160.

[23] M.H. Seymour, Z. Phys. C 62 (1994) 127.

[24] R.P. Feynman, *Photon-Hadron Interactions*. Benjamin, New York, (1972); K.H. Streng, T.F. Walsh and P.M. Zerwas, Z. Phys. C 2 (1979) 237.

[25] ZEUS Coll., S. Chekanov et al., Phys. Rev. D 67 (2003) 012007.

[26] A.D. Martin et al., Eur. Phys. J. C 28 (2003) 455.

[27] J. Pumplin et al., JHEP 0207 (2002) 012;
D. Stump et al., JHEP 0310 (2003) 046.

[28] ZEUS Coll., M. Derrick et al., Phys. Lett. B 293 (1992) 465.

[29] ZEUS Coll., U. Holm (ed.), *The ZEUS Detector*. Status Report (unpublished), DESY (1993), available on `http://www-zeus.desy.de/bluebook/bluebook.html`.

[30] N. Harnew et al., Nucl. Inst. Meth. A 279 (1989) 290;
B. Foster et al., Nucl. Phys. Proc. Suppl. B 32 (1993) 181;
B. Foster et al., Nucl. Inst. Meth. A 338 (1994) 254.

[31] M. Derrick et al., Nucl. Inst. Meth. A 309 (1991) 77;
A. Andresen et al., Nucl. Inst. Meth. A 309 (1991) 101;
A. Caldwell et al., Nucl. Inst. Meth. A 321 (1992) 356;
A. Bernstein et al., Nucl. Inst. Meth. A 336 (1993) 23.

[32] J. Andruszków et al., Preprint DESY-92-066, DESY, 1992;
ZEUS Coll., M. Derrick et al., Z. Phys. C 63 (1994) 391;
J. Andruszków et al., Acta Phys. Pol. B 32 (2001) 2025.

[33] H. Abramowicz, A. Caldwell and R. Sinkus, Nucl. Inst. Meth. A 365 (1995) 508;
R. Sinkus and T. Voss, Nucl. Inst. Meth. A 391 (1997) 360.

[34] S. Bentvelsen, J. Engelen and P. Kooijman, *Proc. of the Workshop on Physics at HERA*, W. Buchmüller and G. Ingelman (eds.), Vol. 1, p. 23. Hamburg, Germany, DESY (1992);
K.C. Höger, ibid., p. 43.

[35] J.E. Huth et al., *Research Directions for the Decade. Proc. of Summer Study on High Energy Physics, 1990*, E.L. Berger (ed.), p. 134. World Scientific (1992). Also in preprint FERMILAB-CONF-90-249-E.

[36] R. Brun et al., GEANT3, Technical Report CERN-DD/EE/84-1, CERN, 1987.

[37] A. Kwiatkowski, H. Spiesberger and H.-J. Möhring, Comp. Phys. Comm. 69 (1992) 155;
H. Spiesberger, *An Event Generator for ep Interactions at HERA Including Radiative Processes (Version 4.6)*, 1996, available on `http://www.desy.de/~hspiesb/heracles.html`.

[38] K. Charchuła, G.A. Schuler and H. Spiesberger, Comp. Phys. Comm. 81 (1994) 381;
H. Spiesberger, HERACLES *and* DJANGOH*: Event Generation for ep Interactions at HERA Including Radiative Processes*, 1998, available on `http://wwwthep.physik.uni-mainz.de/~hspiesb/djangoh/djangoh.html`.

[39] Y. Azimov et al., Phys. Lett. B 165 (1985) 147;
G. Gustafson, Phys. Lett. B 175 (1986) 453;

G. Gustafson and U. Pettersson, Nucl. Phys. B 306 (1988) 746;
B. Andersson et al., Z. Phys. C 43 (1989) 625.

[40] L. Lönnblad, Comp. Phys. Comm. 71 (1992) 15;
L. Lönnblad, Z. Phys. C 65 (1995) 285.

[41] G. Ingelman, A. Edin and J. Rathsman, Comp. Phys. Comm. 101 (1997) 108.

[42] H.L. Lai et al., Eur. Phys. J. C 12 (2000) 375.

[43] B. Andersson et al., Phys. Rep. 97 (1983) 31.

[44] T. Sjöstrand, Comp. Phys. Comm. 82 (1994) 74;
T. Sjöstrand et al., Comp. Phys. Comm. 135 (2001) 238.

[45] T. Sjöstrand, Comp. Phys. Comm. 39 (1986) 347;
T. Sjöstrand and M. Bengtsson, Comp. Phys. Comm. 43 (1987) 367.

[46] S. Catani and M.H. Seymour, Nucl. Phys. B 485 (1997) 291. Erratum in Nucl. Phys. B 510 (1998) 503.

[47] R.K. Ellis, D.A. Ross and A.E. Terrano, Nucl. Phys. B 178 (1981) 421.

[48] S. Bethke, J. Phys. G 26 (2000) R27. Updated in Preprint hep-ex/0606035, 2006.

[49] M. Wing (on behalf of the ZEUS Coll.), *Proc. of the 10th International Conference on Calorimetry in High Energy Physics*, R. Zhu (ed.), p. 767. Pasadena, USA (2002). Also in preprint hep-ex/0206036.

[50] ZEUS Coll., S. Chekanov et al., Eur. Phys. J. C 21 (2001) 443.

[51] R.W.L. Jones et al., JHEP 0312 (2003) 007.

[52] C. Glasman, *Proc. of the 13th International Workshop on Deep Inelastic Scattering*, S.R. Dasu and W.H. Smith (eds.), p. 689. Madison, USA (2005). Also in preprint hep-ex/0506035.

[53] D.J. Gross and F. Wilczek, Phys. Rev. Lett. 30 (1973) 1343;
H.D. Politzer, Phys. Rev. Lett. 30 (1973) 1346;
D.J. Gross and F. Wilczek, Phys. Rev. D 8 (1973) 3633;
H.D. Politzer, Phys. Rep. 14 (1974) 129.

[54] W.E. Caswell, Phys. Rev. Lett. 33 (1974) 244;
D.R.T. Jones, Nucl. Phys. B 75 (1974) 531;
E.S. Egorian and O.V. Tarasov, Theor. Mat. Fiz. 41 (1979) 26.

$E_{T,\mathrm{B}}^{\mathrm{jet}}$ bin (GeV)	$d\sigma/dE_{T,\mathrm{B}}^{\mathrm{jet}}$ (pb/GeV)	δ_{stat}	δ_{syst}	δ_{ES}	C_{QED}	C_{had}
$R = 1$						
8-10	63.98	0.68	$^{+1.20}_{-1.39}$	$^{+2.84}_{-2.56}$	0.95	0.91
10-14	29.29	0.34	$^{+0.37}_{-0.52}$	$^{+1.25}_{-1.31}$	0.96	0.95
14-18	11.07	0.20	$^{+0.15}_{-0.20}$	$^{+0.61}_{-0.50}$	0.96	0.96
18-25	3.234	0.080	$^{+0.036}_{-0.045}$	$^{+0.156}_{-0.167}$	0.94	0.97
25-35	0.773	0.033	$^{+0.016}_{-0.015}$	$^{+0.040}_{-0.033}$	0.95	0.95
35-100	0.0312	0.0027	$^{+0.0005}_{-0.0006}$	$^{+0.0015}_{-0.0022}$	1.06	0.95
$R = 0.7$						
8-10	50.09	0.60	$^{+0.93}_{-1.19}$	$^{+2.16}_{-1.94}$	0.95	0.77
10-14	23.38	0.30	$^{+0.30}_{-0.38}$	$^{+1.11}_{-1.06}$	0.96	0.83
14-18	8.97	0.18	$^{+0.17}_{-0.19}$	$^{+0.47}_{-0.41}$	0.96	0.88
18-25	2.659	0.071	$^{+0.031}_{-0.038}$	$^{+0.120}_{-0.126}$	0.95	0.91
25-35	0.631	0.029	$^{+0.024}_{-0.025}$	$^{+0.028}_{-0.026}$	0.96	0.92
35-100	0.0237	0.0022	$^{+0.0006}_{-0.0007}$	$^{+0.0015}_{-0.0016}$	1.03	0.93
$R = 0.5$						
8-10	38.25	0.52	$^{+0.85}_{-1.11}$	$^{+1.81}_{-1.60}$	0.95	0.64
10-14	17.78	0.26	$^{+0.26}_{-0.30}$	$^{+0.85}_{-0.77}$	0.96	0.70
14-18	7.09	0.15	$^{+0.22}_{-0.23}$	$^{+0.32}_{-0.33}$	0.95	0.77
18-25	2.257	0.063	$^{+0.027}_{-0.032}$	$^{+0.096}_{-0.103}$	0.96	0.83
25-35	0.514	0.025	$^{+0.020}_{-0.020}$	$^{+0.024}_{-0.024}$	0.97	0.86
35-100	0.0208	0.0019	$^{+0.0006}_{-0.0006}$	$^{+0.0014}_{-0.0011}$	1.04	0.90

Table 1: *Inclusive jet cross-sections $d\sigma/dE_{T,\mathrm{B}}^{\mathrm{jet}}$ for jets of hadrons in the Breit frame selected with the longitudinally invariant k_T cluster algorithm for different values of R (Fig. 1). The statistical, uncorrelated systematic and jet-energy-scale (*ES*) uncertainties are shown separately. The multiplicative corrections applied to the data to correct for QED radiative effects, C_{QED}, and the corrections for hadronisation effects to be applied to the parton-level NLO QCD calculations, C_{had}, are shown in the last two columns.*

Q^2 bin (GeV^2)	$d\sigma/dQ^2$ ($\mathrm{pb/GeV}^2$)	δ_{stat}	δ_{syst}	δ_{ES}	C_{QED}	C_{had}
$R = 1$						
125-250	1.106	0.012	$^{+0.013}_{-0.020}$	$^{+0.066}_{-0.062}$	0.97	0.92
250-500	0.3671	0.0053	$^{+0.0048}_{-0.0078}$	$^{+0.0153}_{-0.0149}$	0.95	0.94
500-1000	0.1037	0.0020	$^{+0.0020}_{-0.0021}$	$^{+0.0033}_{-0.0029}$	0.95	0.95
1000-2000	0.02439	0.00072	$^{+0.00039}_{-0.00033}$	$^{+0.00059}_{-0.00058}$	0.94	0.96
2000-5000	0.00396	0.00017	$^{+0.00017}_{-0.00015}$	$^{+0.00008}_{-0.00008}$	0.94	0.95
5000-100000	0.000036	0.000003	$^{+0.000003}_{-0.000003}$	$^{+0.000001}_{-0.000001}$	0.98	0.96
$R = 0.7$						
125-250	0.855	0.010	$^{+0.007}_{-0.012}$	$^{+0.054}_{-0.048}$	0.97	0.79
250-500	0.2913	0.0046	$^{+0.0053}_{-0.0079}$	$^{+0.0124}_{-0.0119}$	0.95	0.83
500-1000	0.0840	0.0018	$^{+0.0017}_{-0.0017}$	$^{+0.0026}_{-0.0024}$	0.95	0.86
1000-2000	0.02079	0.00066	$^{+0.00041}_{-0.00043}$	$^{+0.00046}_{-0.00049}$	0.94	0.88
2000-5000	0.00332	0.00016	$^{+0.00018}_{-0.00016}$	$^{+0.00007}_{-0.00006}$	0.93	0.88
5000-100000	0.000031	0.000003	$^{+0.000002}_{-0.000002}$	$^{+0.000001}_{-0.000001}$	0.97	0.90
$R = 0.5$						
125-250	0.6344	0.0088	$^{+0.0058}_{-0.0092}$	$^{+0.0406}_{-0.0357}$	0.97	0.64
250-500	0.2246	0.0040	$^{+0.0053}_{-0.0069}$	$^{+0.0097}_{-0.0097}$	0.95	0.70
500-1000	0.0672	0.0016	$^{+0.0020}_{-0.0019}$	$^{+0.0021}_{-0.0020}$	0.94	0.75
1000-2000	0.01709	0.00060	$^{+0.00049}_{-0.00051}$	$^{+0.00043}_{-0.00042}$	0.94	0.79
2000-5000	0.00296	0.00015	$^{+0.00016}_{-0.00015}$	$^{+0.00006}_{-0.00006}$	0.95	0.81
5000-100000	0.000028	0.000003	$^{+0.000002}_{-0.000002}$	$^{+0.000001}_{-0.000000}$	0.98	0.83

Table 2: *Inclusive jet cross-sections $d\sigma/dQ^2$ for jets of hadrons in the Breit frame selected with the longitudinally invariant k_T cluster algorithm for different values of R (Fig. 2). Other details as in the caption to Table 1.*

R	$\sigma_{\rm jets}$ (pb)	$\delta_{\rm stat}$	$\delta_{\rm syst}$	$\delta_{\rm ES}$	$C_{\rm QED}$	$C_{\rm had}$
$Q^2 > 125$ GeV^2						
0.5	197.8	1.9	$^{+3.3}_{-4.1}$	$^{+9.3}_{-8.6}$	0.96	0.70
0.7	255.6	2.1	$^{+3.3}_{-4.4}$	$^{+11.9}_{-11.1}$	0.96	0.82
1.0	321.5	2.4	$^{+4.2}_{-5.4}$	$^{+14.8}_{-14.1}$	0.96	0.94
$Q^2 > 500$ GeV^2						
0.5	62.3	1.1	$^{+1.5}_{-1.4}$	$^{+1.7}_{-1.7}$	0.95	0.77
0.7	75.8	1.3	$^{+1.3}_{-1.3}$	$^{+2.1}_{-2.0}$	0.95	0.87
1.0	91.6	1.4	$^{+1.6}_{-1.5}$	$^{+2.6}_{-2.4}$	0.95	0.95

Table 3: *Inclusive jet cross-sections $\sigma_{\rm jets}$ for jets of hadrons in the Breit frame selected with the longitudinally invariant k_T cluster algorithm for $Q^2 > 125$ and 500 GeV^2 (Fig. 3). Other details as in the caption to Table 1.*

$\langle E^{\rm jet}_{T,{\rm B}} \rangle$ (GeV)	α_s	$\delta_{\rm stat}$	$\delta_{\rm syst}$	$\delta_{\rm theor}$
8.9	0.1907	$^{+0.0038}_{-0.0038}$	$^{+0.0194}_{-0.0171}$	$^{+0.0208}_{-0.0192}$
11.7	0.1746	$^{+0.0028}_{-0.0028}$	$^{+0.0123}_{-0.0126}$	$^{+0.0148}_{-0.0142}$
15.7	0.1719	$^{+0.0032}_{-0.0031}$	$^{+0.0105}_{-0.0092}$	$^{+0.0107}_{-0.0105}$
20.7	0.1519	$^{+0.0028}_{-0.0028}$	$^{+0.0061}_{-0.0065}$	$^{+0.0057}_{-0.0057}$
28.6	0.1512	$^{+0.0037}_{-0.0037}$	$^{+0.0050}_{-0.0045}$	$^{+0.0043}_{-0.0044}$
41.2	0.1452	$^{+0.0064}_{-0.0063}$	$^{+0.0041}_{-0.0056}$	$^{+0.0036}_{-0.0036}$

Table 4: *The α_s values determined from a QCD fit of the measured $d\sigma/dE^{\rm jet}_{T,{\rm B}}$ with $R = 1$ as a function of $E^{\rm jet}_{T,{\rm B}}$ (Fig. 4). The statistical, systematic and theoretical uncertainties are shown separately.*

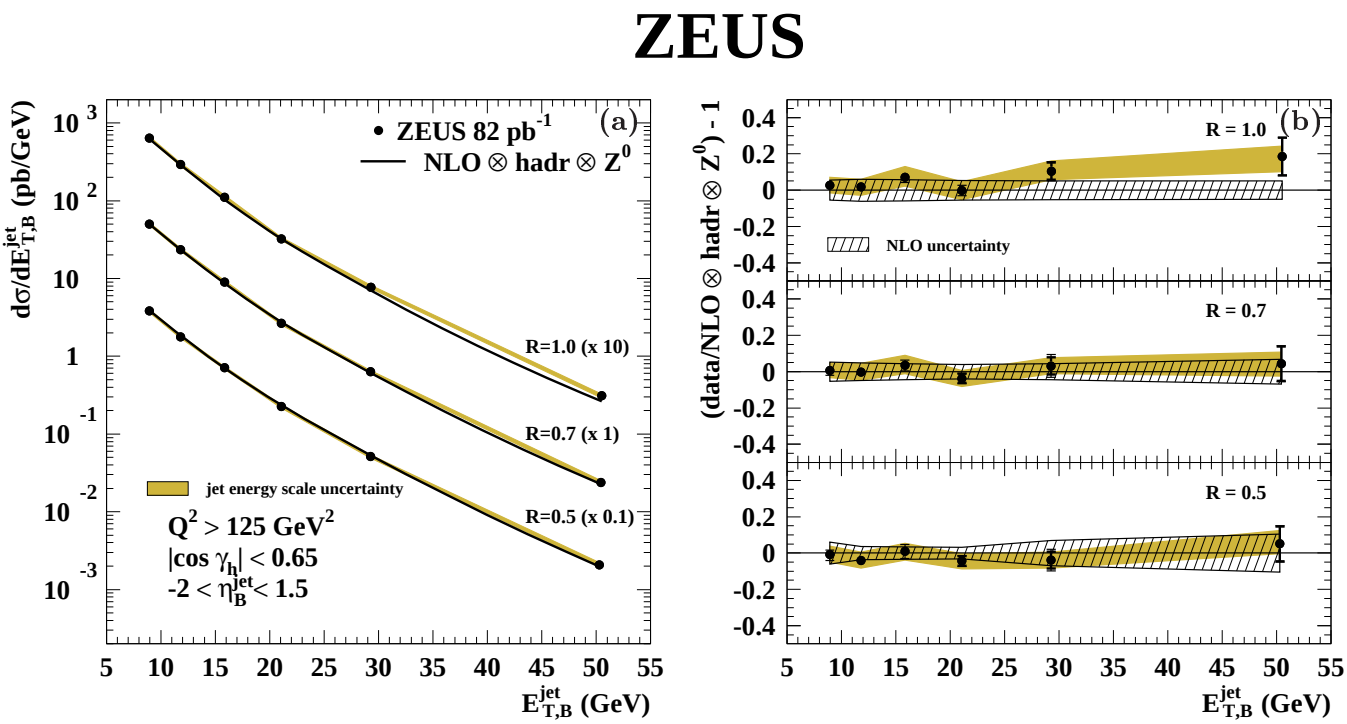

Figure 1: *(a) The measured differential cross-section $d\sigma/dE^{\rm jet}_{T,\rm B}$ for inclusive-jet production with $-2 < \eta^{\rm jet}_{\rm B} < 1.5$ (dots) for different jet radii, in the kinematic range given by $Q^2 > 125$ GeV^2 and $|\cos\gamma_h| < 0.65$. The NLO QCD calculations with $\mu_R = E^{\rm jet}_{T,\rm B}$ (solid lines), corrected to include hadronisation and Z^0 effects and using the ZEUS-S parameterisations of the proton PDFs, are also shown. Each cross section has been multiplied by the scale factor indicated in brackets to aid visibility. (b) The fractional differences between the measured $d\sigma/dE^{\rm jet}_{T,\rm B}$ and the NLO QCD calculations (dots); the hatched bands display the total theoretical uncertainty. The inner error bars represent the statistical uncertainty. The outer error bars show the statistical and systematic uncertainties, not associated with the uncertainty in the absolute energy scale of the jets, added in quadrature. The shaded bands display the uncertainty due to the absolute energy scale of the jets.*

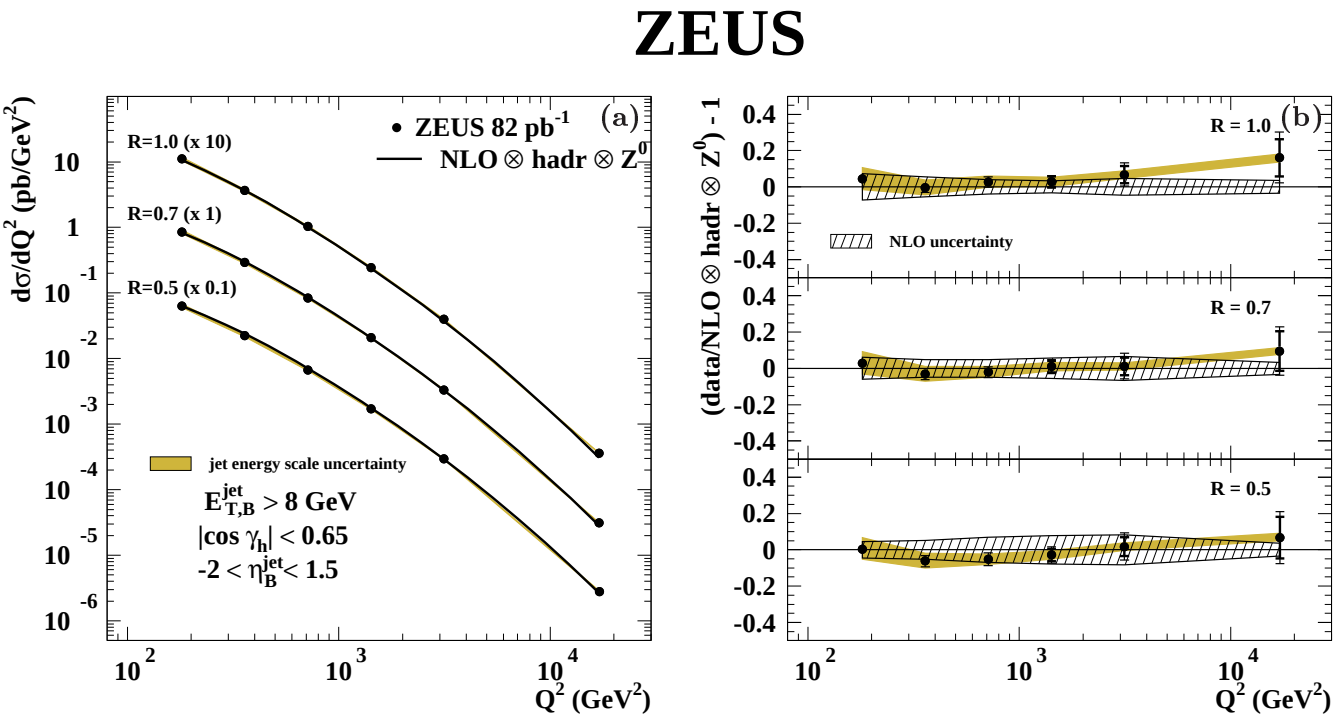

Figure 2: *The measured differential cross-section $d\sigma/dQ^2$ for inclusive-jet production with $E^{\rm jet}_{T,\rm B} > 8$ GeV and $-2 < \eta^{\rm jet}_{\rm B} < 1.5$ (dots) for different jet radii, in the kinematic range given by $|\cos\gamma_h| < 0.65$. Other details as in the caption to Fig. 1.*

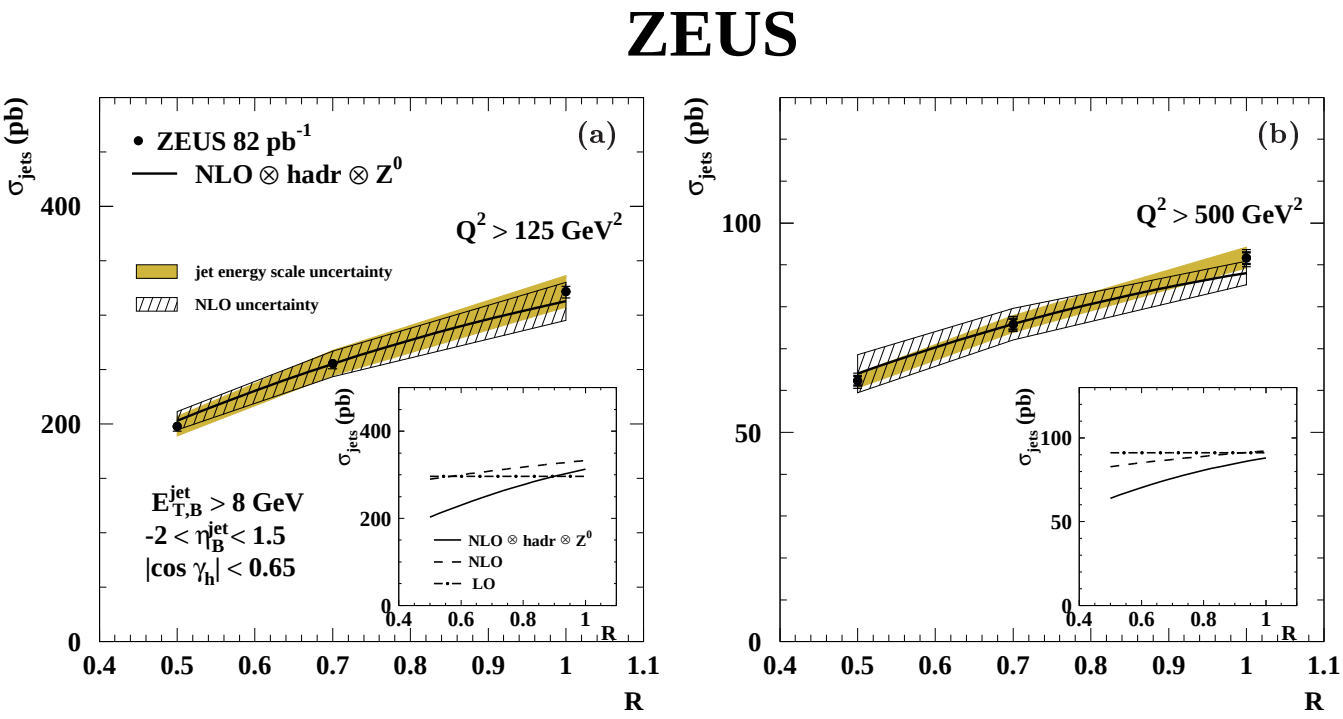

Figure 3: *The measured cross-section $\sigma_{\rm jets}$ as a function of the jet radius for inclusive-jet production with $E^{\rm jet}_{T,{\rm B}} > 8$ GeV and $-2 < \eta^{\rm jet}_{\rm B} < 1.5$ (dots), in the kinematic range given by $|\cos\gamma_h| < 0.65$ and (a) $Q^2 > 125$ GeV^2 and (b) $Q^2 > 500$ GeV^2. The insets show the LO (dot-dashed lines) and NLO (dashed lines) QCD calculations. The NLO QCD calculations corrected to include hadronisation and Z^0 effects are shown as solid lines. Other details as in the caption to Fig. 1.*

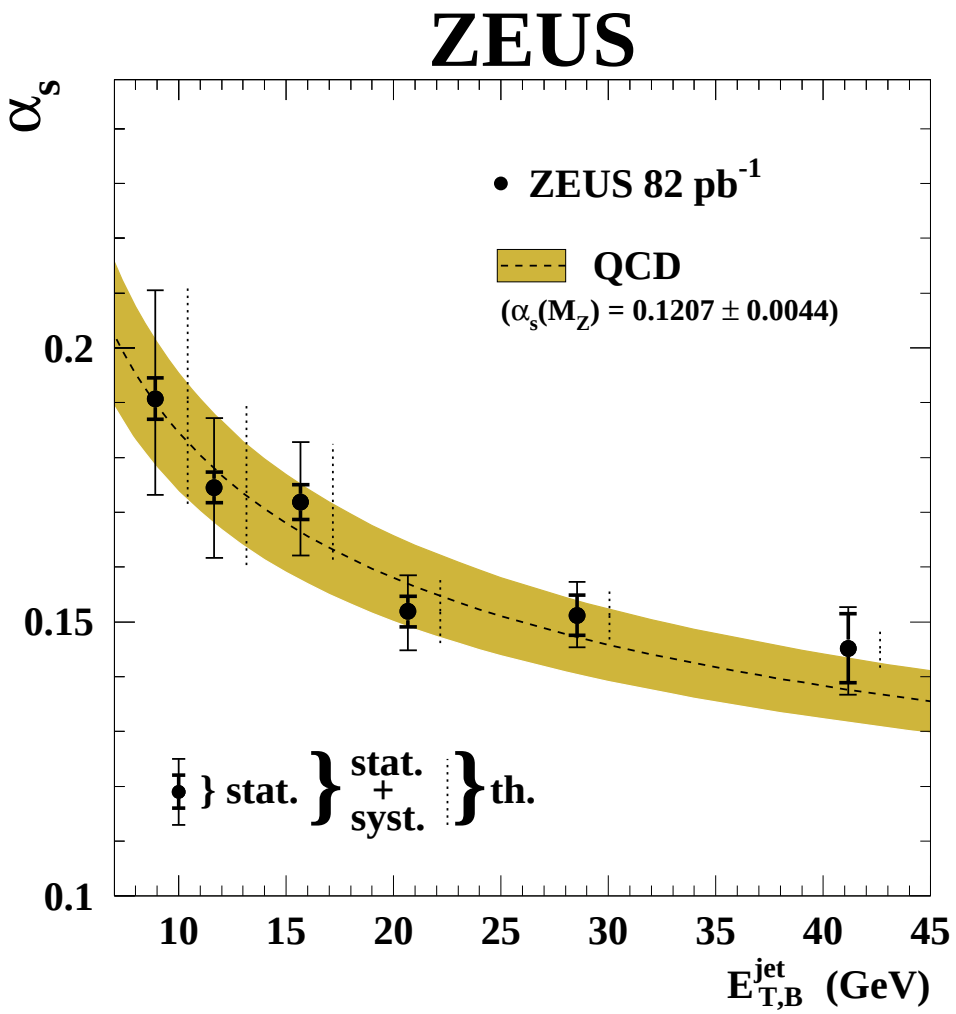

Figure 4: *The α_s values determined from the measured $d\sigma/dE^{\rm jet}_{T,\rm B}$ with $R = 1$ as a function of $E^{\rm jet}_{T,\rm B}$ (dots). The dashed line indicates the renormalisation group prediction at two loops obtained from the $\alpha_s(M_Z)$ value determined in this analysis and the shaded area represents its uncertainty. The inner error bars represent the statistical uncertainties of the data. The outer error bars show the statistical and systematic uncertainties added in quadrature. The dotted vertical bars, shifted to aid visibility, represent the theoretical uncertainties.*